

See discussions, stats, and author profiles for this publication at: <https://www.researchgate.net/publication/276145287>

Photosplitting of Water from Wide-Gap Cu(In,Ga)S₂ Thin Films Modified with a CdS Layer and Pt Nanoparticles for a High-Onset-Potential Photocathode

ARTICLE *in* THE JOURNAL OF PHYSICAL CHEMISTRY C · APRIL 2015

Impact Factor: 4.77 · DOI: 10.1021/acs.jpcc.5b02068

CITATION

1

READS

1,028

7 AUTHORS, INCLUDING:



[Wilman Septina](#)

University of Zurich

32 PUBLICATIONS 201 CITATIONS

[SEE PROFILE](#)



[Ryu Abe](#)

Kyoto University

113 PUBLICATIONS 5,642 CITATIONS

[SEE PROFILE](#)

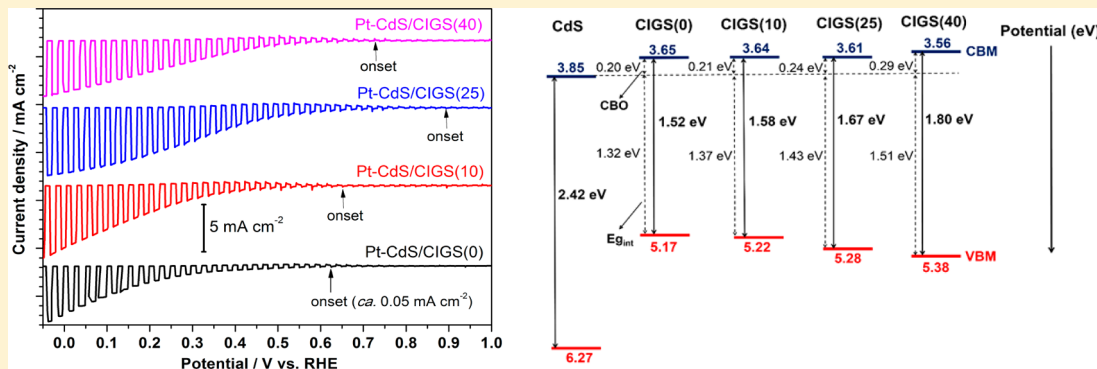
Photosplitting of Water from Wide-Gap Cu(In,Ga)S₂ Thin Films Modified with a CdS Layer and Pt Nanoparticles for a High-Onset-Potential Photocathode

Wilman Septina,[†] Gunawan,[†] Shigeru Ikeda,^{*,†} Takashi Harada,[†] Masanobu Higashi,[‡] Ryu Abe,[‡] and Michio Matsumura[†]

[†]Research Center for Solar Energy Chemistry, Osaka University, 1-3 Machikaneyama, Toyonaka, Osaka 560-8531, Japan

[‡]Department of Energy and Hydrocarbon Chemistry, Graduate School of Engineering, Kyoto University, Katsura Nishikyo-ku, Kyoto 615-8510, Japan

S Supporting Information



ABSTRACT: Photoelectrochemical water splitting from photocathodes based on wide-gap Cu(In,Ga)S₂ (CIGS) thin films modified with a CdS layer and Pt nanoparticles was investigated. CIGS films with various amounts of Ga were fabricated using spray pyrolysis followed by sulfurization. As analyzed using 0.1 M Na₂SO₄ (pH 9) as an electrolyte under illumination of simulated sunlight (AM 1.5G), both photocurrent densities and onset potentials of the photocathodes were gradually improved by an increase in the amount of Ga in the CIGS films up to a Ga/(In + Ga) ratio of 0.25 (Pt-CdS/CIGS(25)). Further inclusion of Ga in the CIGS film was detrimental for both photocurrent density and onset potential. The maximum photocurrent density of 6.8 mA cm⁻² (at 0 V vs RHE) and the highest photocurrent onset potential of 0.89 V vs RHE were obtained by using the Pt-CdS/CIGS(25) photocathode. Achievements of a relatively wide interface band gap of the CIGS/CdS heterointerface and formation of relatively large grains in the Pt-CdS/CIGS(25) sample were likely to be responsible for such superior water reduction properties.

1. INTRODUCTION

Copper chalcopyrite semiconductors of Cu(In,Ga)(S,Se)₂ include a wide range of compounds that are of interest for photoelectrochemical (PEC) water splitting due to their band gaps in the range of 1.0–2.5 eV by varying the alloy ratio. The conduction band of the compounds is also well positioned above the reduction potential of water, enabling them to be used as photocathodes for H₂ generation.^{1–4} Furthermore, chalcopyrite materials generally have a high absorption coefficient, which allows efficient absorption of sunlight by using thin samples.^{5,6} On the basis of achievements of highly efficient solar cells with maximum conversion efficiency of over 21% by using coevaporated Cu(In,Ga)Se₂,⁷ these compounds are expected to have excellent properties as photocathode parts in a tandem system of PEC water splitting.

Important factors required for photocathodes of PEC water splitting are photocurrent (photocurrent density), onset

potential (photovoltage), and stability; i.e., photocathodes having positive onset potentials coupled with high and stable photocurrents are promised in order to induce water splitting by using a tandem system without applied bias energy.^{8,9} For chalcopyrite materials applied to the photocathode part, this could be achieved through band gap engineering by altering the composition of the alloy. Zhang et al. investigated Ag doping to CuGaSe₂, and they found that minor Ag doping to CuGaSe₂ leads to a lower valence band maximum (VBM) of the materials, which resulted in higher onset potential and photocurrent than those of pure CuGaSe₂.¹⁰ More recently, they demonstrated further improvement of the photocurrent and onset potential of the Ag-doped CuGaSe₂ (ACGSe)-based

Received: March 3, 2015

Revised: April 2, 2015

photocathode by deposition of a CuGa₃Se₅ layer on the ACGSe surface.¹¹

In our recent reports, we have shown that CuInS₂-based photocathodes modified with n-type compounds such as CdS and In₂S₃ are able to induce relatively efficient water splitting compared with other chalcopyrite systems.¹² In most cases, modification of p-type photoabsorbers (CuInS₂,^{4,12,13} CuGaSe₂,^{10,11,14} CZTS,^{15,16} GaP₂,¹⁷ Cu₂O,¹⁸ etc.) with a suitable n-type material resulted in significant enhancement of both photocurrent and onset potential of water reduction compared with that of unmodified photoabsorbers. This enhancement was usually explained by formation of a higher built-in field in the semiconductor p-n junction than that at the semiconductor/electrolyte interface: this leads to enhancement of charge separation. In the solar cell field, moreover, addition of Ga to CuInS₂ was found to increase the open-circuit voltage of the solar cell due to widening of the band gap.^{19,20} It is also expected that a similar trend can be observed for the onset potential of this photocathode. Guan et al. demonstrated recently a promising photocurrent from the CdS- and Pt-modified CuIn_{0.7}Ga_{0.3}S₂ nanophotocathode, though its onset potential needs to be further improved.²¹

In the present study, we investigated the impact of controlled addition of various amounts of Ga to the CuInS₂ thin film on structural, electrical, and morphological properties of the film. The spray pyrolysis method was used for fabrication of these chalcopyrite films due to its low cost and easiness of compositional controls; i.e., film compositions can be controlled effectively by adjusting the concentrations of the constituents in the precursor solution. PEC water splitting properties were investigated after modification of the films with CdS layers and Pt nanoparticles. We found that there was a significant improvement in both photocurrent and onset potential when Cu(In,Ga)S₂ (CIGS) with an optimal amount of Ga was used as the photoactive layer compared with those of the Ga-free CuInS₂ film.

2. EXPERIMENTAL SECTION

Fabrication of Cu(In,Ga)S₂ Thin Films. Four CIGS precursor films with different amounts of Ga were fabricated by varying the molar ratio of Ga/(Ga + In) in the solution (0, 0.10, 0.25, and 0.40). Aqueous solutions containing 0.09 M Cu(NO₃)₂, 0.1 M of a mixture of In(NO₃)₃ and Ga(NO₃)₃ with different Ga/(Ga + In) ratios, and 0.8 M thiourea (SC(NH₂)₂) were sprayed on an Mo-coated glass substrate heated at 370 °C with a spray rate of 0.67 cm³ min⁻¹ by using a homemade spray deposition apparatus. Nitrogen (N₂) gas was used as a carrier gas during the deposition. The thus-obtained films were sulfurized in the presence of 5 mg of elemental sulfur powder in an evacuated Pyrex ampule at 600 °C for 10 min. Thus-obtained CIGS films are labeled CIGS(Ga/(Ga + In) ratio).

Surface Modification with CdS Layers. Surface modification of the prepared CIGS films by CdS layers was performed by the chemical bath deposition (CBD) method. In a typical deposition procedure, CIGS films were immersed in an aqueous solution containing 12.5 mM CdSO₄, 0.22 M SC(NH₂)₂, and 11 M NH₄OH for 7 min. CBD was performed at 60 °C. The sample was then rinsed thoroughly with distilled water. The deposition resulted in the formation of ca. 50–80 nm thick CdS layers on CIGS films (labeled CdS/CIGS).

Surface Modification with Pt. Pt particles were deposited on the CdS/CIGS film by photoelectrodeposition. The

deposition was performed by using a three-electrode system consisting of the CdS/CIGS sample as a working electrode, a Pt wire as a counter electrode, and Ag/AgCl as a reference electrode. These electrodes were immersed in 0.1 M Na₂SO₄ solution containing 1 mM H₂PtCl₆, and the deposition was performed with a constant potential of -0.1 V for 10 min by using a Solartron SI1280B electrochemical measurement unit. During the deposition, the CdS/CIGS working electrode was illuminated by simulated AM 1.5 solar irradiation from an Asahi Spectra HAL320 solar simulator. Typical current-time response for the Pt deposition is shown in Figure S1 (Supporting Information); successful deposition of Pt on CdS/CIGS was confirmed from X-ray photoelectron spectroscopy (XPS), as shown in Figure S2 (Supporting Information). Thus-obtained CdS/CIGS modified with Pt was labeled Pt-CdS/CIGS.

Photoelectrochemical Measurements. The same three-electrode setup as that used for the Pt deposition (see above) was used for PEC measurements of the Pt-CdS/CIGS photocathode. PEC H₂ generation from the photocathode was examined in 0.1 M Na₂SO₄ solution electrolyte with pH adjusted to 9. The above-mentioned solar simulator was used as a light source. Potentials referred to the Ag/AgCl electrode were converted to reversible hydrogen electrode (RHE) using the Nernst equation as follows

$$E_{\text{RHE}} = E_{\text{Ag/AgCl}} + 0.059 \times \text{pH} + 0.199$$

The half-cell solar-to-hydrogen efficiency (HC-STH) was determined from the *J*-V response of the photocathodes by using the following equation^{11,13}

$$\text{HC-STH} (\%) = J \times (V - V_{\text{H+}/\text{H2}}) \times 100\% / P$$

where *J* is photocurrent density (mA cm⁻²); *V* is applied potential (V vs RHE); *V_{H+}/_{H2}}* is the equilibrium redox potential of hydrogen (0 V vs RHE); and *P* is intensity of simulated sunlight (100 mW cm⁻²).

Incident photon to current efficiency (IPCE) of the photocathodes was also obtained by recording the photocurrent of samples illuminated by a monochromatic light of variable wavelength chopped at a frequency of 10 Hz. The number of incident photons was determined with an OPHIR Orion Laser power meter equipped with a photodiode detector. IPCE was calculated using the following equation

$$\text{IPCE} (\%) = 1240 \times J_{\text{ph}} \times 100 / (\lambda \times P)$$

where *J_{ph}* is photocurrent density of the sample recorded using the lock-in technique at the respective wavelength of light (λ) at 0 V (vs RHE) using an NF LI5630 digital lock-in amplifier connected to a Hokuto Denko HAB-151 potentiogalvanostat.

A PEC cell connected to an online gas chromatography system (INFICON 3000 Micro GC Gas Analyzer equipped with an MS-5A column and a thermal conductivity detector) was used to detect H₂ and O₂ during the PEC water splitting. The PEC cell was immersed in a water bath to maintain the temperature at 288 K, and photoirradiation was performed at 0 V (vs RHE) by using a Cermax LX-300F 300 W xenon lamp.

Characterizations of Fabricated CIGS Films. Crystalline structures of the films were determined by X-ray diffraction (XRD) using a Rigaku Mini Flex X-ray diffractometer (Cu K α , Ni filter). Elemental compositions of the films were determined using a Hitachi TM3000 scanning electron microscope (SEM) equipped with a SwiftED3000 energy-dispersive X-ray spec-

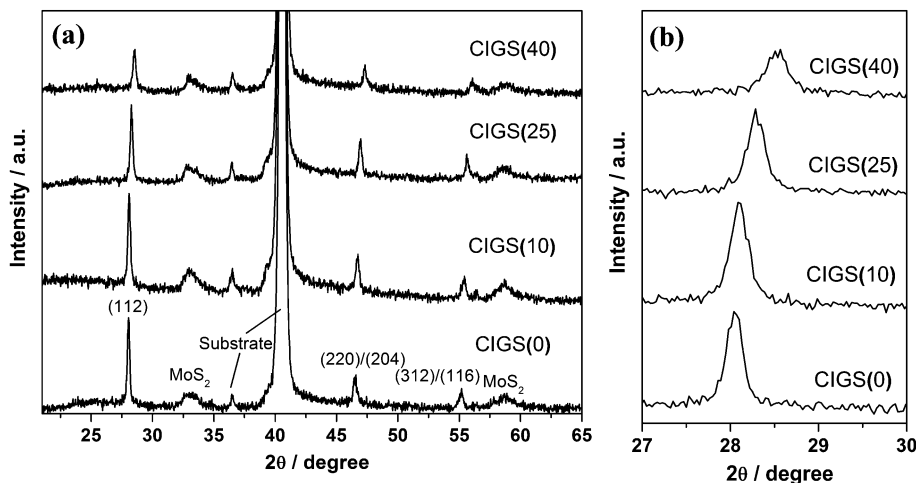


Figure 1. (a) XRD patterns of CIGS(0), CIGS(10), CIGS(25), and CIGS(40) after sulfurization and (b) magnified view of (112) diffraction planes.

trometer (EDX). Morphologies of the films were examined by field emission scanning electron microscopy (FE-SEM) using a Hitachi S-5000 FEG scanning electron microscope. Ionization potentials of CIGS films were analyzed by photoelectron spectroscopy (PES) using a Riken Keiki AC-3 surface analyzer. Surface structures of Pt-CdS/CIGS films were examined by X-ray photoelectron spectroscopy (XPS) using a Shimadzu AXIS ULTRA X-ray photoelectron spectrometer.

3. RESULTS AND DISCUSSION

3.1. Effect of Amount of Ga on CIGS on Structural and Morphological Properties. Figure 1a shows XRD patterns of sulfurized CIGS precursor films with various amounts of Ga in the precursor films. The main peaks of the sulfurized film with no Ga (i.e., CIGS(0)) were observed at 2θ of 28.0°, 46.6°, and 55.2°, and they are assignable to the (112), (220)/(204), and (312)/116 reflections of CuInS₂ with a chalcopyrite structure (JCPDS 27-0159). With an increase in the Ga content in the film, gradual shifts of those peaks to higher angles were observed, as shown in Figure 1b for the shift of the (112) peak. Observations of these gradual shifts of diffraction peaks revealed effective incorporation of Ga into the In atomic site to form the mixed crystal Cu(In,Ga)S₂ (CIGS), instead of formation of separate phases of CuInS₂ and CuGaS₂. Comparable intensities and fwhm of (112) peaks of CIGS(0), CIGS(10), and CIGS(25) films (0.22°, 0.23°, and 0.22°, respectively) indicate their similar degrees of crystallinity, whereas CIGS(40) showed a less intense (112) reflection and a wider fwhm (0.26°). Broad peaks observed at 2θ of 33° and 58.8° derived from MoS₂ were also observed for all films, indicating partial sulfurization of the bottom Mo layer. The atomic compositions of these CIGS films measured by EDX are summarized in Table 1. The Ga/(Ga + In) ratios of the sulfurized films were close to the intended Ga/(Ga + In) ratios in precursor solutions.

Effects of Ga content on morphologies of CIGS films were also investigated. Figure 2 shows cross-sectional and surface SEM images of CIGS films with various Ga contents. All of the films have comparable thickness of around 550 nm regardless of the Ga content. At the interface between the CIGS film and the bottom Mo layer, the formation of an MoS₂ layer with thicknesses ranging from 470 to 550 nm was confirmed in all films in agreement with the previous XRD results. Although the cross-sectional images of these films shown in Figures 2a–d did

Table 1. Elemental Composition of Thus-Obtained Sulfurized CIGS Films Obtained from Various Ga/(Ga + In) Ratios in the Precursor Solution

Ga/(Ga + In) ratio in the solution	Cu (% at.)	In (% at.)	Ga (% at.)	S (% at.)	Ga/(Ga + In) in the films
0	24.45	25.19	0	50.36	0
0.10	25.61	22.84	1.94	49.61	0.08
0.25	26.21	16.88	5.40	51.51	0.24
0.40	25.18	13.24	9.80	51.78	0.42

not show obvious differences between the samples with different Ga contents, the corresponding surface SEM images showed distinctive differences, as can be seen in Figure 2e–h: the CIGS(0) and CIGS(10) films consisted of densely packed small grains with sizes of 50 nm. On the other hand, the CIGS(25) film was composed of distinctive columnar grains and had larger grain sizes than those of the CIGS(0) film (ca. 100–200 nm). When the Ga content was increased to $\text{Ga}/(\text{Ga} + \text{In}) = 0.4$, crystalline grains of the film (CIGS(40)) became slightly inhomogeneous; i.e., the film was seen to consist of irregular grains when compared to those of the other films. These results were consistent with observations of relatively low intensity of the (112) reflection of the CIGS(40) film in the above XRD results (see Figure 1).

3.2. PEC Properties of CdS and Pt-Modified CIGS Photocathodes. For PEC water-splitting analysis, the CIGS films with different Ga contents were modified with CdS layers by CBD followed by deposition of Pt (Pt-CdS/CIGS). Figure 3 shows typical surface SEM images of a Pt-CdS/CIGS(25) photocathode. When compared to the bare CIGS(25) surface, the morphology of the Pt-CdS/CIGS(25) surface was completely different. The appearance of densely packed granular grains on the entire surface indicates homogeneous coverage of the CdS layer. Pt was deposited as nanoparticles of a few ten nanometers in size on the granular grains: these particles were well dispersed on the CdS-covered CIGS layer. XPS analysis of the Pt-CdS/CIGS(25) sample also indicated the existence of CdS and Pt on the CIGS film (Figure S2, Supporting Information). In addition, no XPS signal assignable to Cu 2p appeared in the XPS spectrum of the Pt-CdS/CIGS(25) sample, indicating homogeneous coverage with the CdS layer on top of the CIGS(25) layer.

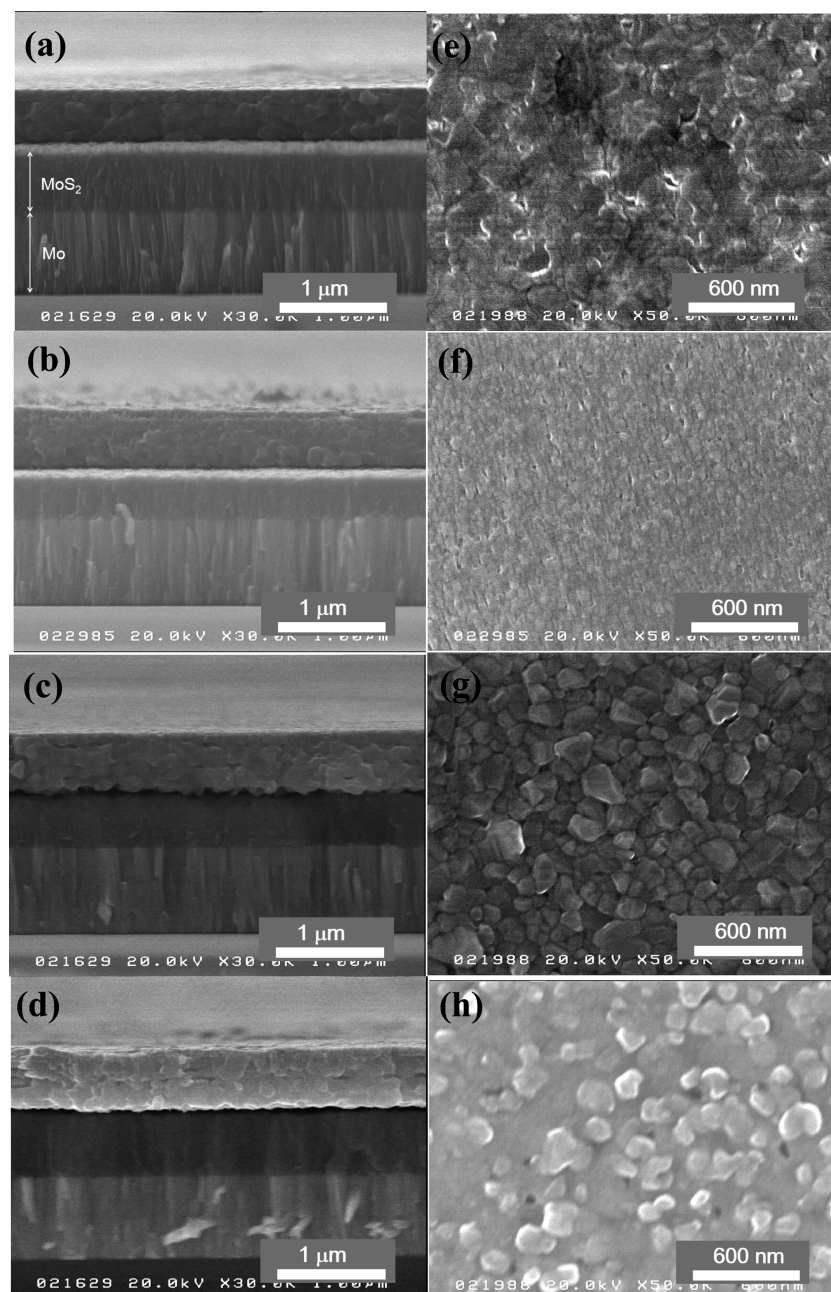


Figure 2. SEM images of (a),(e) CIGS(0), (b),(f) CIGS(10), (c),(g) CIGS(25), and (d),(h) CIGS(40).

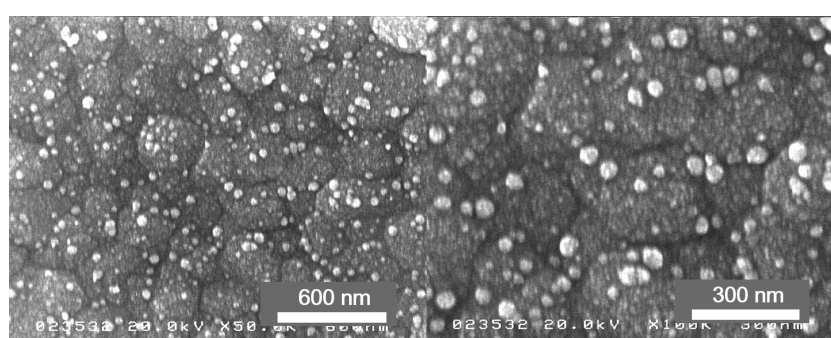


Figure 3. SEM images of Pt-CdS/CIGS(25) with various magnifications.

Figure 4 shows current density–voltage (J – V) curves of the fabricated photocathodes measured at 0.1 M Na_2SO_4 (pH 9)

swept in the anodic direction from the potentials of -0.1 to 1.0 V (vs RHE) under chopped illumination from AM 1.5

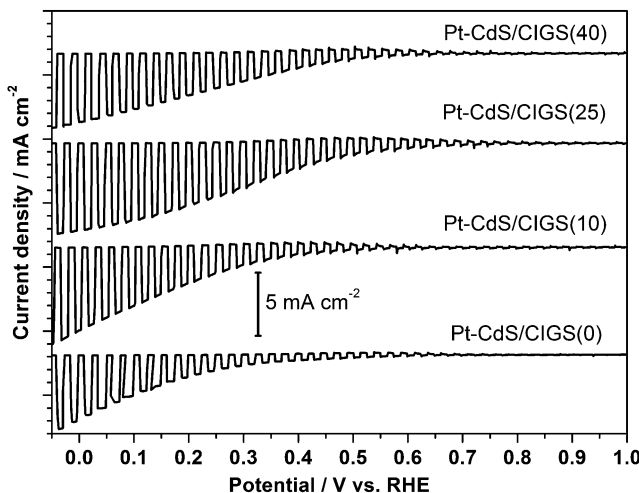


Figure 4. J – V curves of Pt-CdS/CIGS electrodes with different Ga contents measured in 0.1 M Na_2SO_4 (pH 9) under chopped illumination from AM 1.5 simulated solar irradiation.

simulated sunlight. All of the samples showed cathodic photocurrents due to reduction of water into H_2 . Table 2

Table 2. Compilation of the Photocurrent Density at 0 V vs RHE and Onset Potential (i.e., Leading Potential Showing 0.05 mA cm⁻² of Cathodic Photocurrent) of the Pt-CdS/CIGS Photocathodes Measured in 0.1 M Na_2SO_4 (pH 9) under Chopped Illumination from AM 1.5 Simulated Solar Irradiation

CIGS samples	photocurrent density at 0 V vs RHE (mA cm ⁻²)	onset potential (vs RHE)
CIGS(0)	5.21	0.62
CIGS(10)	6.24	0.65
CIGS(25)	6.78	0.89
CIGS(40)	5.49	0.73

summarizes photocurrent densities at 0 V (vs RHE) and onset potentials of several Pt-CdS/CIGS samples with different Ga contents. It should be noted that the onset potential was defined as the leading potential showing 0.05 mA cm⁻² of cathodic photocurrent. Gradual increases in onset potentials and cathodic photocurrent densities were observed up to $\text{Ga}/(\text{Ga} + \text{In}) = 0.25$ (Pt-CdS/CIGS(25) sample): the Pt-CdS/CIGS(25) photocathode had the highest onset potential and the largest cathodic photocurrent density at 0 V vs RHE. In addition, when half-cell solar-to-hydrogen efficiency (HC-STH) of the Pt-CdS/CIGS(25) photocathode was calculated from J – V curves, the sample showed maximum HC-STH of 1.1% at 0.28 V (vs RHE) (Figure S3, Supporting Information). This is the best performance in the present system, and further increment of the Ga content was detrimental for both onset potential and photocurrent density.

In order to study further properties of the photocathodes, IPCE spectra of the photocathodes were measured at 0 V vs RHE, and the results are shown in Figure 5. The highest IPCE maximum of 30% was obtained from Pt-CdS/CIGS(25), as expected from the above PEC results. It is clear from the figure that onsets of IPCE spectra shifted to shorter wavelength regions with increase in the Ga content, indicating widening of band gap energies. By deformations of these spectra into $[-h\nu \ln(1 - \text{IPCE})]^2$ vs $h\nu$ (eV) plots at onset regions and applying

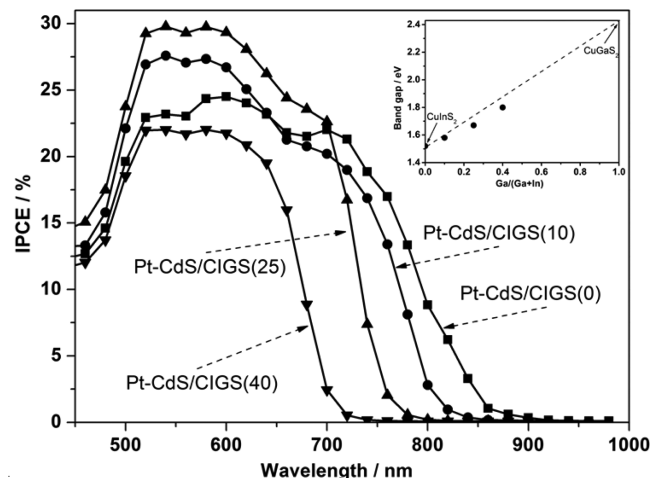


Figure 5. IPCE of Pt-CdS/CIGS using CIGS with various amounts of Ga measured in 0.1 M Na_2SO_4 (pH 9) at 0 V vs RHE. Inset shows a plot of band gaps (eV) of the present CIGS as a function of $\text{Ga}/(\text{Ga} + \text{In})$ (dotted shape), with the dashed line (---) indicating theoretical estimation of the band gap of CIGS based on a linear relationship with the amount of Ga.

extrapolation to the energy axis, band gap energies of the CIGS(0), CIGS(10), CIGS(25), and CIGS(40) samples were estimated to be 1.52, 1.58, 1.67, and 1.80 eV, respectively (Figure S4, Supporting Information). Since In-free CuGaS₂ has a band gap energy of ca. 2.43 eV,²² there would be a linear relationship between band gap energies and Ga contents in the present CIGS system, as shown in the inset of Figure 5. Another point worth noting is that steep decreases in IPCEs at a wavelength lower than 520 nm were observed in all of the samples due to the absorption of light by the CdS layer.²³

3.3. Band Alignment of CdS/CIGS. In order to investigate the effect of Ga content in the CIGS films on their valence band maximum (VBM) and conduction band minimum (CBM) positions, photoelectron spectroscopy (PES) measurements were performed. Figure 6 shows typical PES spectra of CIGS films with different Ga contents. The spectrum of Au was also taken as a reference (Figure S5, Supporting Information): the estimated work function is 4.82 eV, which is in agreement with the reported value.²⁴ It is clear that onsets of these spectra gradually shifted toward a large binding energy region with increase in the Ga content, indicating deepening of VBMs by replacement of the In site with Ga in CIGS. A similar trend was also observed in photocurrent measurements of the CIGS films in an $\text{Eu}(\text{NO}_3)_3$ redox electrolyte solution; i.e., gradual positive shifts of cathodic photocurrents were observed with an increase in the Ga content (Figure S6, Supporting Information). This trend was somewhat different from the reported effect of Ga on its selenide counterpart $\text{Cu}(\text{In},\text{Ga})\text{Se}_2$ (CIGSe) system. In the case of CIGSe, it is thought that an increase of Ga leads to only a slight decrease of VBM, while the CBM was significantly increased.^{25,26} There have been limited experimental systematic studies on the effect of Ga on the sulfide case. Therefore, further experimental and theoretical studies are required to determine the precise role of Ga in the band structure of CIGS.

For quantitative comparison, energy positions of VBMs of the CIGS films were deduced from extrapolation of the PES spectra. By combining with the band gap values determined from the above IPCE spectra, VBMs and CBMs of the CIGS films were estimated as shown in Figure 7. We also determined

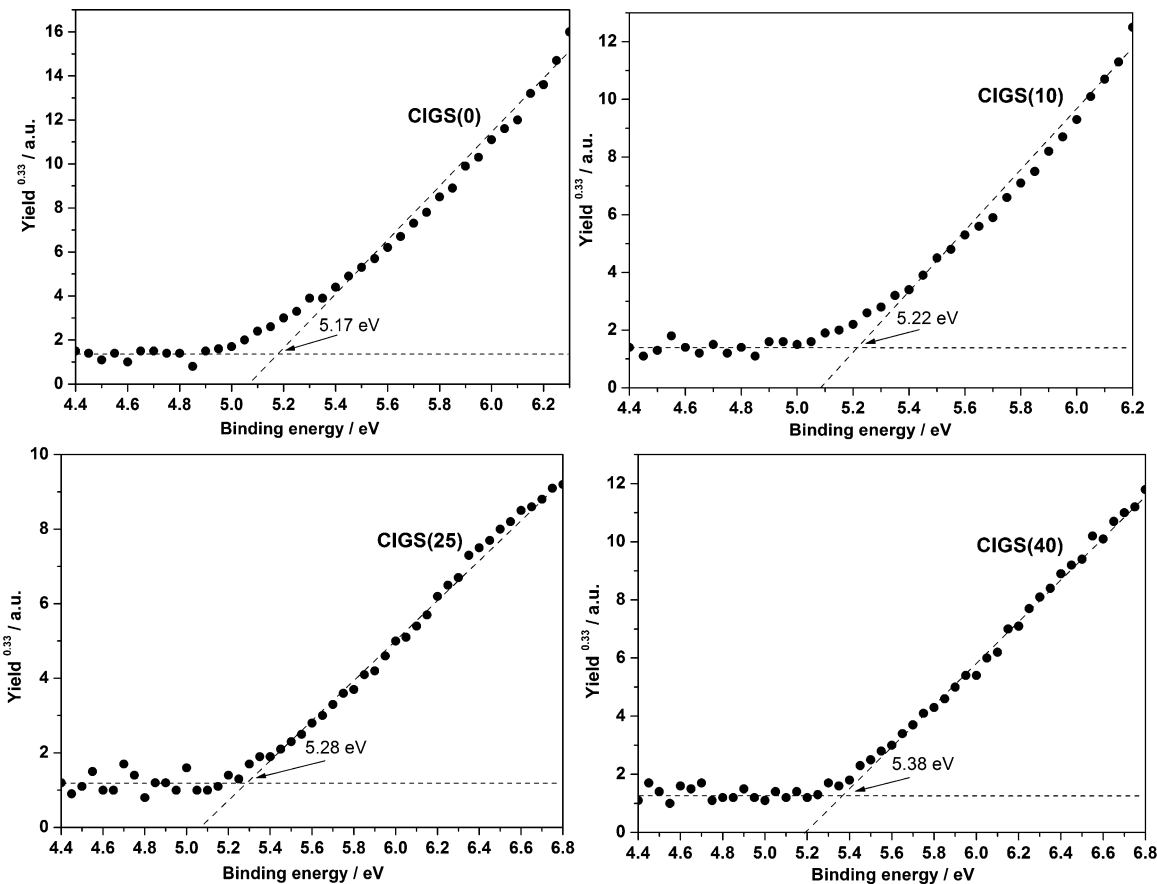


Figure 6. PES spectra of CIGS with different amounts of Ga. The VBM position of the respected CIGS films can be estimated from the extrapolation of the curves toward the baseline.

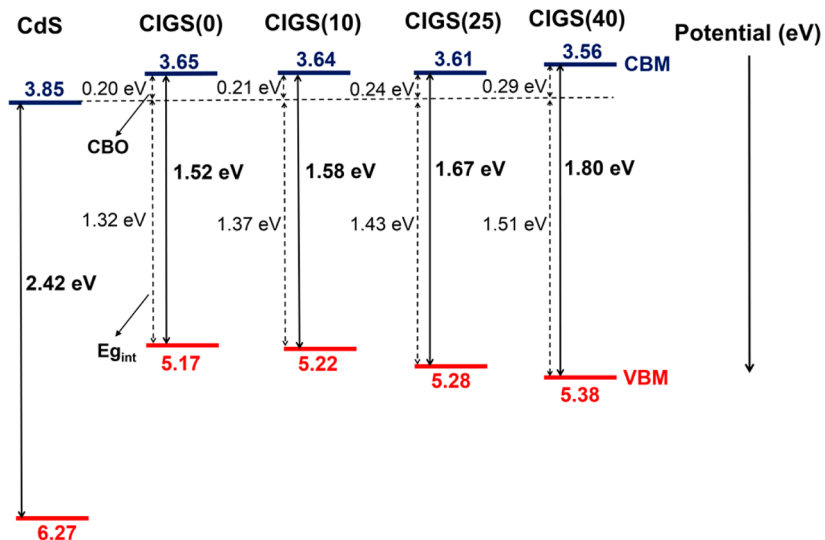


Figure 7. Band positions of CIGS with a different amount of Ga. Relative band position of CdS was also shown as a comparison including conduction band offset (CBO) and interface band gap ($E_{g\text{int}}$) of the CdS/CIGS junctions.

relative band positions of the CIGS films with CdS by measuring the valence band offset of CdS/CIGS(0) as a reference with XPS via Ar etching from the surface through the junction (Figure S7, Supporting Information). As shown in Figure S7 (Supporting Information), the conduction band offset (CBO) of the CdS/CIGS(0) junction was estimated to be ca. 0.2 eV in a cliff-type alignment. Such a cliff-type

alignment was in agreement with several reports regarding the CdS/CuInS₂ heterojunction.^{27–29} Since only slight upward shifts of CBMs were induced by partial substitution of In with Ga in the present CIGS system, CBO values did not change significantly regardless of the Ga content in the CIGS films. On the other hand, the energy differences between VBMs of CIGS films and the CBM of the CdS layer, defined as interface band

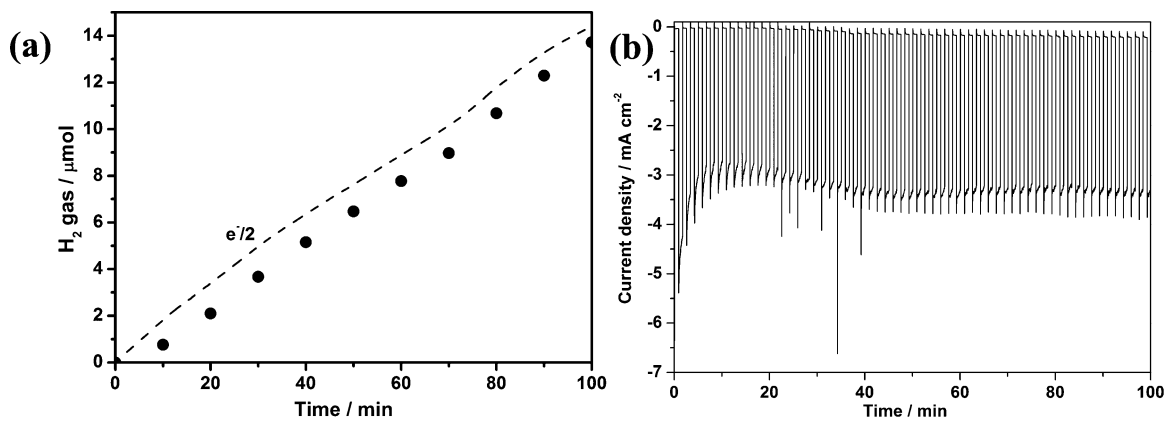


Figure 8. (a) Time course H₂ gas evolution from the Pt-CdS/CIGS(25) measured at 0.1 M Na₂SO₄ (pH 9) at 0 V vs RHE measured using illumination from 300 W xenon. The dashed line denotes a time course curve of half of the electrons passing through the outer circuit (e⁻/2). (b) Photocurrent–time profile of Pt-CdS/CIGS(25) measured at 0.1 M Na₂SO₄ (pH 9) using chopped illumination from an AM 1.5 solar simulator.

gap ($E_{g_{int}}$'s), were appreciably enlarged by increasing in the Ga content in the CIGS films. Both CBO and $E_{g_{int}}$ should be important parameters when analyzing the potential limit of photovoltage of a p–n junction. In the solar cell field, it is widely believed that the junction of the Cu(In,Ga)S₂ system with CdS is not optimal due to the cliff-type alignment (CBO < 0 eV) which enhanced the interface recombination rate due to cross recombination of photogenerated electrons from the CBM of CdS with holes at the VBM of Cu(In,Ga)S₂.²⁹ Because of the comparable CBO values of the present CIGS samples with different Ga contents, such influence of the negative CBO value was likely to be the same between these samples. Since $E_{g_{int}}$ values corresponded to built-in potentials of the p–n junction, the expected photovoltage should depend strongly on this parameter. Hence, observation of a relatively positive photocurrent onset for the Pt-CdS/CIGS(25) sample compared to those observed for Pt-CdS/CIGS(0) and Pt-CdS/CIGS(10) samples is attributed to the larger $E_{g_{int}}$ value of Pt-CdS/CIGS(25) than those of Pt-CdS/CIGS(0) and Pt-CdS/CIGS(10).

While the above explanation could be true for the onset potential gain up to the Ga content of 0.25 (Pt-CdS/CIGS(25)), the onset potential was negatively shifted when using the Pt-CdS/CIGS(40) sample. The replacement of a large number of In with Ga is likely to be associated with increment of midgap states and/or defect states, which act as trap sites of photogenerated carriers, thus leading to limiting photovoltage. As discussed above, the low crystalline quality of CIGS(40) compared to that of the other films (see Figure 1) as well as the formation of inhomogeneous surface morphology of this film (see Figure 2h) indicate deterioration of the p–n junction property. Indeed, the superior photocurrent and onset potential of the photocathode using CIGS(25) could be highly influenced by its relatively large grain sizes as it would facilitate smoother charge transport, whereas small grain sizes would promote a high density of grain boundaries throughout the film which would enhance charge recombination.

3.4. H₂ Gas Liberation Activity and Stability of the Photocathode. Figure 8a shows a time course of H₂ gas liberation activity over Pt-CdS/CIGS(25) using the three-electrode setup at 0 V (vs RHE) under illumination from a 300 W xenon lamp. The produced H₂ increased monotonically with time and reached ca. 13.7 μmol at 100 min. The amount of evolved H₂ significantly exceeded the molar amount of

Cu(In,Ga)S₂, which was approximately 0.06 μmol assuming the density is equal to that of CuInS₂ (4.6 g cm⁻³) with an area of 0.06 cm². The faradic efficiency, defined as the ratio in percent of the amount of H₂ evolution to that of half electrons passing through the outer circuit (e⁻/2) after 100 min photoirradiation, was estimated to be 95%.

A typical photocurrent stability profile of Pt-CdS/CIGS under constant applied bias of 0 V (vs RHE) with chopped illumination is shown in Figure 8b. The photocurrent initially showed rapid decay up to about 10 min, and then it showed a slight increase up to about 40 min and was relatively stable over the observed time course. Decay of the photocurrent with time for CdS-modified photocathodes was reported by several authors^{10,13} as well as by our group.¹² Zhao et al. attributed the decay to poor stability of CdS caused by photocorrosion.¹³ To improve the photostability of the photocathode, they added a TiO₂ protective layer on the top of CdS, which resulted in a significant enhancement of stability of the photocurrent over a 1 h period. In our previous report, we also showed that In₂S₃-modified CuInS₂ had better photocurrent stability than that of the CdS-modified one. Therefore, efforts to improve the photocurrent stability by use of a protective layer or alternative n-type layers are now being made.

4. CONCLUSION

Cu(In,Ga)S₂ films with various amounts of Ga (Ga/(Ga + In) of 0, 0.1, 0.25, and 0.4) were fabricated by the spray pyrolysis method followed by sulfurization. The amount of Ga in CIGS affected the morphology of the film with larger grain size being obtained for CIGS with a Ga/(Ga + In) ratio of 0.25. After modification with a CdS layer by CBD followed by photoelectrodeposition of Pt nanoparticles, water splitting activity with 0.1 M Na₂SO₄ (pH 9) was examined. Both photocurrent (at 0 V vs RHE) and onset potential of the photocathode were gradually improved up to a Ga/(Ga + In) ratio of 0.25 (Pt-CdS/CIGS(25)); relatively high onset potential of 0.89 V vs RHE was obtained. To our understanding, this onset potential is among the highest for sulfide chalcopyrite-based photocathodes.

■ ASSOCIATED CONTENT

● Supporting Information

Typical current–time profile for photodeposition of Pt on CdS/CIGS, typical wide XPS spectrum of Pt-CdS/CIGS, HC-

STH spectrum of Pt-CdS/CIGS(25), $[-h\nu \ln(1 - \text{IPCE})]^2$ vs band gap (eV) plots of Pt-CdS/CIGS, PES spectrum of Au, photocurrent–potential curves of CIGS with different amount of Ga measured using 0.2 M Eu(NO₃)₃ as the electrolyte with the lock-in technique including the relative flat-band potential of the CIGS, and relative VBM positions of CdS/CIS junction measured by XPS. This material is available free of charge via the Internet at <http://pubs.acs.org>.

■ AUTHOR INFORMATION

Corresponding Author

*E-mail: siked@chem.es.osaka-u.ac.jp.

Notes

The authors declare no competing financial interest.

■ ACKNOWLEDGMENTS

This work was also supported by a Grant-in-Aid for Scientific Research on Innovative Areas (All Nippon Artificial Photosynthesis Project for Living Earth) from MEXT Japan and the A-step feasibility study program from JST Japan. Professor Kazunari Domen and Dr. Tsutomu Minegishi (The University of Tokyo) are gratefully acknowledged for their help in PES measurements.

■ REFERENCES

- (1) Fernandez, A.; Dheree, N.; Turner, J.; Martinez, A.; Arriaga, L.; Cano, U. Photoelectrochemical Characterization of The Cu(In,Ga)S₂ Thin Film Prepared by Evaporation. *Sol. Energy Mater. Sol. Cells* **2005**, *85*, 251–259.
- (2) Marsen, B.; Cole, B.; Miller, E. L. Photoelectrolysis of Water Using Thin Copper Gallium Diselenide Electrodes. *Sol. Energy Mater. Sol. Cells* **2008**, *92*, 1054–1058.
- (3) Yokoyama, D.; Minegishi, T.; Maeda, K.; Katayama, M.; Kubota, J.; Yamada, A.; Konagai, M.; Domen, K. Photoelectrochemical Water Splitting Using a Cu(In,Ga)Se₂ Thin Film. *Electrochem. Commun.* **2010**, *12*, 851–853.
- (4) Ikeda, S.; Nakamura, T.; Lee, S. M.; Yagi, T.; Harada, T.; Minegishi, T.; Matsumura, M. Photoreduction of Water by Using Modified CuInS₂ Electrodes. *ChemSusChem* **2011**, *4*, 262–268.
- (5) Niki, S.; Contreras, M.; Repins, I.; Powalla, M.; Kushiya, K.; Ishizuka, S.; Matsubara, K. CIGS Absorbers and Processes. *Prog. Photovoltaics: Res. Appl.* **2010**, *18*, 453–466.
- (6) Minoura, S.; Kodera, K.; Maekawa, T.; Miyazaki, K.; Niki, S.; Fujiwara, H. Dielectric Function of Cu(In,Ga)Se₂-Based Polycrystalline Materials. *J. Appl. Phys.* **2013**, *113*, 063505.
- (7) Jackson, P.; Hariskos, D.; Wuerz, R.; Kiowski, O.; Bauer, A.; Friedlmeier, T. M.; Powalla, M. Properties of Cu(In,Ga)Se₂ Solar Cells with New Record Efficiencies up to 21.7%. *Phys. Status Solidi RRL* **2015**, *9*, 28–31.
- (8) Walter, M. G.; Warren, E. L.; McKone, J. R.; Boettcher, S. W.; Mi, Q.; Santori, E. A.; Lewis, N. S. Solar Water Splitting Cells. *Chem. Rev.* **2010**, *110*, 6446–6473.
- (9) Prévot, M. S.; Sivula, K. Photoelectrochemical Tandem Cells for Solar Water Splitting. *J. Phys. Chem. C* **2013**, *117*, 17879–17893.
- (10) Zhang, L.; Minegishi, T.; Kubota, J.; Domen, K. Hydrogen Evolution from Water Using Ag_xCu_{1-x}GaSe₂ Photocathodes Under Visible Light. *Phys. Chem. Chem. Phys.* **2014**, *16*, 6167–6174.
- (11) Zhang, L.; Minegishi, T.; Nakabayashi, M.; Suzuki, Y.; Seki, K.; Shibata, N.; Kubota, J.; Domen, K. Durable Hydrogen Evolution from Water Driven by Sunlight using (Ag,Cu)GaSe₂ Photocathodes Modified with CdS and CuGa₃Se₅. *Chem. Sci.* **2015**, *6*, 894–901.
- (12) Gunawan; Septina, W.; Ikeda, S.; Harada, T.; Minegishi, T.; Domen, K.; Matsumura, M. Platinum and Indium Sulfide-Modified CuInS₂ as Efficient Photocathodes for Photoelectrochemical Water Splitting. *Chem. Commun.* **2014**, *50*, 8941.
- (13) Zhao, J.; Minegishi, T.; Zhang, L.; Zhong, M.; Gunawan; Nakabayashi, M.; Ma, G.; Hisatomi, T.; Katayama, M.; Ikeda, S.; et al. Enhancement of Solar Hydrogen Evolution from Water by Surface Modification with CdS and TiO₂ on Porous CuInS₂ Photocathodes Prepared by an Electrodeposition-Sulfurization Method. *Angew. Chem., Int. Ed. Engl.* **2014**, *53*, 11808–12.
- (14) Moriya, M.; Minegishi, T.; Kumagai, H.; Katayama, M.; Kubota, J.; Domen, K. Stable Hydrogen Evolution from CdS-Modified CuGaSe₂ Photoelectrode under Visible-Light Irradiation. *J. Am. Chem. Soc.* **2013**, *135*, 3733–3735.
- (15) Yokoyama, D.; Minegishi, T.; Jimbo, K.; Hisatomi, T.; Ma, G. J.; Katayama, M.; Kubota, J.; Katagiri, H.; Domen, K. H₂ Evolution from Water on Modified Cu₂ZnSnS₄ Photoelectrode under Solar Light. *Appl. Phys. Express* **2010**, *3*, 101202.
- (16) Guijarro, N.; Prévot, M. S.; Sivula, K. Enhancing the Charge Separation in Nanocrystalline Cu₂ZnSnS₄ Photocathodes for Photoelectrochemical Application: The Role of Surface Modifications. *J. Phys. Chem. Lett.* **2014**, 3902–3908.
- (17) Malizia, M.; Seger, B.; Chorkendorff, I.; Vesborg, P. C. K. Formation of a p-n Heterojunction on GaP Photocathodes for H₂ Production Providing an Open-Circuit Voltage of 710 mV. *J. Mater. Chem. A* **2014**, *2*, 6847–6853.
- (18) Paracchino, A.; Laporte, V.; Sivula, K.; Grätzel, M.; Thimsen, E. Highly Active Oxide Photocathode for Photoelectrochemical Water Reduction. *Nat. Mater.* **2011**, *10*, 456–461.
- (19) Merdes, S.; Abou-Ras, D.; Mainz, R.; Klenk, R.; Lux-Steiner, M. C.; Meeder, A.; Schock, H. W.; Klaer, J. CdS/Cu(In,Ga)S₂ based Solar Cells with Efficiencies Reaching 12.9% Prepared by a Rapid Thermal Process. *Prog. Photovoltaics: Res. Appl.* **2013**, *21*, 88–93.
- (20) Ikeda, S.; Nonogaki, M.; Septina, W.; Gunawan, G.; Harada, T.; Matsumura, M. Fabrication of CuInS₂ and Cu(In,Ga)S₂ Thin Films by a Facile Spray Pyrolysis and Their Photovoltaic and Photoelectrochemical Properties. *Catal. Sci. Technol.* **2013**, *3*, 1849.
- (21) Guan, Z.; Luo, W.; Feng, J.; Tao, Q.; Xu, Y.; Wen, X.; Fu, G.; Zou, Z. Selective Etching of Metastable Phase Induced an Efficient CuIn_{0.7}Ga_{0.3}S₂ Nano-Photocathode for Solar Water Splitting. *J. Mater. Chem. A* **2015**, DOI: 10.1039/C5TA01259G.
- (22) Jaffe, J. E.; Zunger, A. Anion Displacements and The Band-Gap Anomaly in Ternary ABC₂ Chalcopyrite Semiconductors. *Phys. Rev. B* **1983**, *27*, 5176–5179.
- (23) Subba Ramaiyah, K.; Pilkington, R. D.; Hill, A. E.; Tomlinson, R. D.; Bhatnagar, A. K. Structural and Optical Investigations on CdS Thin Films grown by Chemical Bath Technique. *Mater. Chem. Phys.* **2001**, *68*, 22–30.
- (24) Anderson, P. A. Work Function of Gold. *Phys. Rev.* **1959**, *115*, 553.
- (25) Wei, S.-H.; Zhang, S.; Zunger, A. Effects of Ga Addition to CuInSe₂ on Its Electronic, Structural, and Defect Properties. *Appl. Phys. Lett.* **1998**, *72*, 3199–3201.
- (26) Zhang, S. B.; Wei, S.-H.; Zunger, A. A Phenomenological Model for Systematization and Prediction of Doping Limits in II-VI and I-III-VI₂ Compounds. *J. Appl. Phys.* **1998**, *83*, 3192–3196.
- (27) Hashimoto, Y.; Takeuchi, K.; Ito, K. Band Alignment at CdS/CuInS₂ Heterojunction. *Appl. Phys. Lett.* **1995**, *67*, 980–982.
- (28) Weinhardt, L.; Fuchs, O.; Groß, D.; Storch, G.; Umbach, E.; Dhere, N. G.; Kadam, A. A.; Kulkarni, S. S.; Heske, C. Band alignment at The CdS/Cu(In,Ga)S₂ Interface in Thin-Film Solar Cells. *Appl. Phys. Lett.* **2005**, *86*, 062109.
- (29) Scheer, R. Open Questions After 20 years of CuInS₂ Research. *Prog. Photovoltaics: Res. Appl.* **2012**, *20*, 507–511.